Published in final edited form as:
*Acad Radiol*. 2008 October ; 15(10): 1246–1254. doi:10.1016/j.acra.2008.03.019.

# METABOLIC AND VASCULAR FEATURES OF DYNAMIC CONTRAST ENHANCED BREAST MRI AND $^{15}$O-WATER PET BLOOD FLOW IN BREAST CANCER

**Peter R. Eby, MD**[1], **Savannah C. Partridge, PhD**[1], **Steven W. White**[1], **Robert K. Doot, MS**[2,3], **Lisa K. Dunnwald, MPH**[2], **Erin K. Schubert, BS**[2], **Brenda F. Kurland, PhD**[4], **Constance D. Lehman, MD, PhD**[1], and **David A. Mankoff, MD, PhD**[1,2]

1*Department of Radiology, University of Washington, Seattle Cancer Care Alliance, 825 Eastlake Avenue East, Seattle, WA 98109-1023*

2*Division of Nuclear Medicine, University of Washington Medical Center, 1959 NE Pacific, Seattle, WA 98195*

3*Department of Bioengineering, University of Washington, Seattle, WA 98195*

4*Clinical Research Division, Fred Hutchinson Cancer Research Center, 1100 Fairview Ave N, Seattle, WA 98109*

## Abstract

**RATIONALE AND OBJECTIVES—**To (1) describe associations between measures of tumor perfusion by dynamic contrast-enhanced breast MRI (DCE-MRI), blood flow by $^{15}$O-water PET and metabolism by $^{18}$F-FDG PET and (2) improve our understanding of tumor enhancement on MRI through independent measures of tumor metabolism and blood flow.

**MATERIALS AND METHODS—**We performed a retrospective analysis of the existing PET and MRI databases from the departments of Nuclear Medicine and Radiology. We identified patients with locally advanced breast cancer who underwent $^{15}$O-water/$^{18}$F-FDG PET within 1 month of clinical DCE-MRI between February 2004 and August 2006. The $^{15}$O-water PET blood flow and $^{18}$F-FDG metabolic rate (MR) and tissue transport constant ($K_1$) in the primary malignancy were calculated. DCE-MRI peak percent enhancement (PE) and peak signal enhancement ratio (SER) were measured for each tumor. Correlations and regression analysis of these variables were performed.

**RESULTS—**Fifteen patients with complete PET and DCE-MRI data were included in the analysis cohort. Peak SER correlated significantly with blood flow (r=0.73, p=0.002) and $K_1$ (r=0.76, p=0.001). However, peak SER did not correlate significantly with FDG MR (r=0.44, p=0.101). There were no significant correlations between peak PE and any of the PET parameters.

**CONCLUSIONS—**Our findings suggest that tumor perfusion, represented by $^{15}$O-water PET blood flow, is an important factor in the MRI enhancement of LABC. A lack of correlation of FDG MR

Address Correspondence To: Peter R. Eby MD, Assistant Professor of Radiology, University of Washington School of Medicine, Seattle Cancer Care Alliance, 825 Eastlake Ave. E., G3-200, Seattle, WA 98109-1023, Phone: (206) 288-1257, Fax: (206) 288-2054, Email: preby@u.washington.edu.

with blood flow and DCE-MRI kinetics suggests that $^{18}$F-FDG PET provides complementary metabolic information independent of vascular factors.

## Introduction

Locally advanced breast cancer (LABC) is most frequently treated by neoadjuvant systemic therapy prior to definitive surgical resection. Dynamic contrast enhanced breast magnetic resonance imaging (DCE-MRI) and positron emission tomography (PET) have been used to evaluate response to traditional cytotoxic neo-adjuvant chemotherapy (1–14). In addition, there is growing interest in targeted breast cancer therapy, such as anti-angiogenic agents, for which non-invasive imaging may be particularly advantageous for response evaluation (3,15–17)

Prior studies have examined DCE-MRI and PET functional studies independently. DCE-MRI defines the extent of breast cancer in vivo more accurately than any other imaging modality (18). In addition, DCE-MRI data can provide measurements of tumor volume and enhancement kinetics. Changes in tumor volume following neoadjuvant therapy, as measured using DCE-MRI, are predictive of recurrence free survival (8). Measurements of tumor enhancement, including semi-quantitative parameters such as initial percent enhancement (PE) and delayed signal enhancement ratio (SER), have been shown to be helpful and accurate for tumor detection and response evaluation (19–26). Tumor enhancement likely reflects a combination of blood flow and capillary permeability (15,27). However, the precise biologic factors underlying enhancement and the relative contributions of blood flow and capillary permeability are not completely understood.

$^{18}$F-fluorodeoxyglucose (FDG) PET has also been widely studied in the setting of neoadjuvant breast cancer therapy (2,4–6,11,12). Changes in glucose metabolism by FDG PET have been shown to predict response to treatment following a single cycle of chemotherapy (28,29). PET measures of tumor perfusion have also been helpful for response assessment through dynamic imaging with $^{15}$O-water, a test that can provide an independent and quantitative measure of blood flow in breast cancer (30,31). Changes in blood flow following neoadjuvant therapy, as quantified by $^{15}$O-water PET, predict pathologic response and disease free survival (5,6,11, 32). Recent studies comparing $^{15}$O-water and FDG PET have shown that the delivery of FDG, measured by the kinetic parameter FDG $K_1$, and blood flow measured by $^{15}$O-water PET are highly correlated, suggesting that blood flow is an important factor in FDG delivery (11,32). These results and the increased use of imaging to monitor therapy motivate an investigation of the relationship between DCE-MRI parameters, PET measures of blood flow and PET FDG kinetics to better understand their relationships and the nature of DCE-MRI kinetic parameters.

Prior studies have examined the relationship between DCE-MRI and FDG PET in predicting response for breast cancer (2,9,10,33). Pilot studies have been performed to validate the correlation of $^{15}$O-water PET blood flow with MRI in the brain, prostate and coronary arteries (34–36). PET blood flow and DCE-MRI kinetic parameters have not been directly compared or correlated in the breast. In addition to a better understanding of the determinants of MRI contrast enhancement, comparing DCE-MRI and $^{15}$O-water PET may improve our ability to predict therapeutic response and provide insights into the mechanisms of anti-angiogenic therapies through quantitative regional differences in blood flow and capillary permeability.

There were two purposes of this study: To (1) test the correlations between DCE-MRI initial percent enhancement (PE) and delayed signal enhancement ratio (SER) with $^{15}$O-water PET blood flow and $^{18}$F-FDG PET metabolic rate (MR) and tissue transport constant ($K_1$) and (2) improve our understanding of DCE-MRI tumor enhancement through independent measures of tumor metabolism and blood flow. Based upon our studies correlating blood flow and metabolism by PET, we hypothesized that, in LABC, DCE-MRI kinetics (peak PE and peak

SER) would directly correlate with measures of tumor perfusion, including blood flow, as measured by $^{15}$O-water PET and FDG $K_1$ (11). We performed an exploratory retrospective study to test this hypothesis.

## Materials and Methods

### Case/patient selection

Our institutional review board approved this Health Insurance Portability and Accountability Act compliant study. The PET database contains patients with LABC receiving neoadjuvant chemotherapy that were enrolled in IRB-approved studies of blood flow and metabolism with monitoring of tumor response via combined $^{15}$O-water/$^{18}$F-FDG PET examinations. Patients within the database were eligible for the study. We identified 35 consecutive patients who underwent at least one combined $^{15}$O-water/$^{18}$F-FDG PET examination over a period of 30 months from February 1, 2004 through August 31, 2006. We then compared this list to the MRI database that includes all patients who underwent a bilateral DCE-MRI between January 2003 and the present. We identified all patients who had a DCE-MRI within one month of the PET examination. We then reviewed clinical information via the institutional electronic medical record system to determine the dates of diagnosis, initiation of chemotherapy, surgery and recurrence. Patients were excluded from the analysis if any portion of the data from the PET or DCE-MRI examinations were incomplete. Patients were also excluded if the time between the PET and DCE-MRI examinations exceeded 1 month or if neoadjuvant therapy was given at any time between the examinations.

### MRI Acquisition Protocols

The clinical breast MRI scanning technique at our institution was optimized for accurate detection and staging, providing images with high spatial resolution, good quality fat suppression, and full bilateral coverage. All study examinations were performed on a GE LX 1.5T scanner (General Electric Medical Systems, Milwaukee, WI) using a dedicated bilateral breast coil. Two different acquisition protocols were employed during the 31 months comprising this study. Each imaging protocol included a bilateral axial localizer sequence, one pre- and at least 3 post-contrast T1-weighted fat suppressed acquisitions. Omniscan (GE) was used for all examinations.

From February 2004 through September 2005 a seven channel phased array receive-only breast coil was used (MRI Devices Excite 7 Channel Biopsy Breast Array) with the GE Volume Imaging for Breast Assessment (VIBRANT) parallel imaging technique (GE). T1-weighted 3D FSPGR imaging parameters were TR = 6.7 ms, TE = 4.2 ms, and flip angle of 10°. Three sequential bilateral post-contrast sagittal acquisitions, lasting 90 seconds each, were centered at 90, 180, and 270. From October 2005 through June 2006 an eight channel phased array receive-only breast coil (GE) was used with the GE VIBRANT parallel imaging technique. Five simultaneous bilateral axial post-contrast acquisitions, lasting 90 seconds each, were centered at 90, 180, 270, 360 and 450 seconds. No other MRI examinations were performed on study patients after June 2006.

### MRI Image Analysis

A data processing software tool was written for use with ImageJ (NIH, public domain), to measure tumor volume and enhancement kinetics on DCE-MRI. Several parameters reflecting contrast enhancement behavior of the tumor were calculated, including the initial percent enhancement (PE), delayed signal enhancement ratio (SER), and washout fraction, as described previously (20,21,37). PE characterizes the height of the enhancement curve at 1.5 minutes and reflects the rate of contrast uptake in the lesion. SER characterizes the shape of the enhancement curve in the delayed phase (after 1.5 minutes) and is proportional to the rate of

contrast washout in the tumor. PE was calculated for each voxel using the pre-contrast ($S_0$) and first post-contrast ($S_1$) sequences according to the following equation:

$$PE = \frac{S_1 - S_0}{S_0} \times 100\% \quad \text{Eq. 1}$$

A threshold of 50% was applied to select significantly enhancing voxels from the PE map and SER was then calculated for each voxel according to the equation:

$$SER = \frac{S_1 - S_0}{S_2 - S_0} \quad \text{Eq. 2}$$

where S2 is the value of the post-contrast sequence centered at 270 seconds. SER values model the shape of the enhancement curve for each voxel with SER > 1.1 indicating washout, SER between 1.1 and 0.9 indicating plateau enhancement, and SER < 0.9 indicating persistent enhancement. SER was previously shown to reflect both micro-vessel density and tumor grade (19,20,24).

An SER map was produced with a maximum threshold of 4 to exclude spurious values that may result from system noise. Axial and sagittal maximum intensity projections (MIPs) were created to allow the radiologist to define the tumor region of interest (ROI). PE and SER values were automatically computed for 'hotspot' or peak regions in each tumor, defined by at least 8 contiguous voxels that produced the highest mean PE and highest mean SER in the tumor. These two values were defined as peak PE and peak SER and used for the data analysis and correlations. Tumor volume was calculated by summing all voxels exceeding the 50% PE threshold. All the data was written to an output file, which was later imported into Excel for data processing.

## PET Acquisition Protocol

Each patient in the data set was enrolled in a study of PET imaging and neoadjuvant therapy for LABC and underwent at least one $^{15}$O-water/$^{18}$F-FDG PET examination according to the University of Washington Human Subjects Committee guidelines. The data from some of these examinations have been previously published along with a description of the experimental protocol (5,6,11). It is summarized here.

PET images were obtained on an Advance Tomograph (GE Medical Systems, Waukesha, WI) with 35 transaxial planes, 4.25 mm thick. Images were corrected for random coincidences, scatter, and attenuation. Image reconstruction was performed by filtered backprojection with a Hanning filter using a 35 × 128 × 128 image matrix and yielded a reconstructed spatial resolution of approximately 10–12 mm. Imaging was performed using 960–2000 MBq (26–54 mCi) of $^{15}$O-water and a two-minute infusion of 260–407 MBq (7–11 mCi) of $^{18}$F-FDG. Glucose concentrations were checked immediately prior to administration of $^{18}$F-FDG (range = 60–170 mg/dL; mean = 93 mg/dL). Dynamic images were obtained for 7.75 min for $^{15}$O-water and 60 min for $^{18}$F-FDG. The dynamic imaging sequence for $^{15}$O-water was 15 × 2 s, 15 × 5 s, 12 × 10 s, 8 × 15 s, and 6 × 20 s. The imaging sequence for $^{18}$F-FDG was 4 × 20 s, 4 × 40 s, 4 × 1 min, 4 × 3 min and 8 × 5 min.

## PET imaging analysis

Tumor regions of interest (ROI) were drawn as 1.5 cm diameter circles on the $^{18}$F-FDG images around the area of maximum tumor activity over three contiguous planes chosen to be the most biologically aggressive portion of the tumor as previously described(11). The blood clearance curve was obtained from a left ventricular ROI.

### Kinetic Models

The $^{15}$O-water analysis used a single tissue compartment model described by Wilson et al to estimate tumor blood flow (mL/min/g) and water distribution volume (mL/g) (30,38). For this study, blood flow was used for primary correlation with DCE-MRI data.

The $^{18}$F-FDG analysis used a two tissue compartment model described by Phelps et al and Reivich et al and modified from Reivich et al to incorporate decay of the radiotracer as described in Tseng et al 2004 (11,39–41). From FDG compartmental analysis FDG transport [$K_1$, mL/min/g] and the FDG metabolism flux constant [$K_i$, mL/min/g] were selected for comparison to the DCE-MRI parameters. As in our prior studies, the metabolic rate of FDG (FDG MR, μmole/min/100g), reflecting the rate of glucose consumption, was calculated as

$$\text{FDG MR} = [\text{Glucose}]^{*}K_i$$

where [Glucose] is the plasma glucose concentration (μmole/mL) at the time of FDG PET. We have previously examined the relationship between FDG $K_1$ and FDG MR and blood flow measured by $^{15}$O-water PET and to response to therapy (11).

### Statistical Analysis

Data for each patient were entered into a spreadsheet (Excel, Microsoft, Redmond, WA). Pearson product-moment correlation coefficients and linear regression models were calculated between DCE-MRI parameters of peak SER and peak PE with PET parameters of $^{15}$O-water blood flow, $^{18}$F-FDG MR and $K_1$, and tumor size using JMP software (SAS Institute, Cary, NC) and R version 2.5.0 (R Foundation for Statistical Computing, Vienna, Austria). Two-sided P values <.05 were considered significant.

## Results

Fifteen patients with paired DCE-MRI and $^{15}$O-water/$^{18}$F-FDG PET examinations (13 pre-therapy and 2 post-therapy) met all study inclusion criteria and comprise the analysis set. Figure 1 depicts the PET and DCE-MRI examinations in a single study patient. The PET and DCE-MRI examinations were performed between 0 and 20 days apart (median 8.0 days). Tumor volume ranged from 2.1 – 147.1 cc (median 25.8 cc).

Bivariate scatterplots of DCE-MRI peak SER and PET variables are shown in Figure 2. The panels with fitted lines graphically represent the significant positive linear relationships between peak SER and blood flow (Figure 2A, r=0.73, p=0.002) and peak SER and $K_1$ (Figure 2C, r=0.76, p=0.001). A single patient with the highest peak SER (2.29) and PET blood flow (0.75 mL/min/g) and $K_1$ (0.25 mL/min/g) appeared to have high leverage in estimating the associations among DCE-MRI and PET measures. A sensitivity analysis removing this point reduced the correlations (from r=0.73 to 0.5, and from r=0.76 to 0.59 respectively) but the linear fit (dashed lines in Figure 2A and 2C) did not significantly change.

Peak SER and FDG MR did not correlate significantly (Figure 2B, r=0.44, p=0.101). Peak PE did not demonstrate significant correlations with any of the PET parameters: blood flow r=0.28, p=0.304, FDG MR r=0.15, p=0.589 and $K_1$ r=0.30, p=0.277 (Table 1).

Blood flow, $K_1$, and peak SER were all positively correlated with tumor volume. In addition, positive associations remained with peak SER for both blood flow (p=0.032) and $K_1$ (p=0.028) in multivariable linear regression controlling for tumor volume. Fitted values for these relationships for the median tumor volume of 25.8 cc are shown as dotted lines in Figures 2A and 2C.

Correlations between the $^{15}$O-water PET and $^{18}$F-FDG PET variables are shown in Figure 3. Blood flow did not significantly correlate with FDG MR (Figure 3A, r=0.37, p=0.17). Blood flow correlated significantly with $K_1$ (Figure 3B, r=0.87, p=<0.0001). Removing the high-leverage data point resulted in a different linear fit (dashed line in Figure 3B) and smaller estimated correlation (r=0.76, p=0.002).

## Discussion

This retrospective analysis of a unique data set in patients with LABC includes PET $^{15}$O-water blood flow, $^{18}$F-FDG MR and $K_1$ and DCE-MRI peak SER and peak PE. The analysis allows a comparison of independent measures of the rate of delivery of different molecules ($^{15}$O-water, $^{18}$F-FDG and a gadolinium based MRI contrast agent) to locally advanced breast tumors in vivo. The associations between PET and MRI measures may lead to a better understanding of angiogenesis, vascular permeability, and glucose transport in LABC and to improvements in our ability to interpret changes seen on the imaging modalities in response to therapy. Our findings indicate that vascular supply, represented by $^{15}$O-water PET blood flow, is an important factor in the enhancement of LABC on MRI.

We found strong to moderate correlations of peak SER with blood flow and peak SER with $K_1$. The strong correlation between blood flow and peak SER supports the hypothesis that DCE-MRI kinetics are heavily influenced by tumor blood flow. SER reflects the change in enhancement 90 seconds after contrast injection. Values of SER less than 1 indicate a persistent increase in enhancement over time. Values of SER greater than 1 indicate decreasing delayed enhancement (i.e. washout). Prior work published by Kuhl et al indicates that masses in the breast with washout on DCE-MRI are more likely malignant (23). Higher values of peak SER are strongly correlated with high blood flow in our study. However, the correlation is not perfect which suggests that enhancement is multi-factorial. Pham et al and Knopp et al have hypothesized that the enhancement observed on MRI is a combination of vascular supply and vascular permeability (15,27).

Unlike water, which is nearly freely diffusible through tissues, FDG and Gadolinium-based MRI contrast agents (Gd) are molecules that are affected by capillary permeability. They differ in that Gd enters the extracellular space, but not the intracellular space, whereas FDG reaches the intracellular space via glucose transporters. It is therefore interesting to speculate that DCE-MRI kinetic parameters and FDG $K_1$ might correlate closely for conditions where glucose membrane transport is not rate-limiting, but might differ under circumstances where glucose transporters are perturbed, such as has been suggested for certain targeted therapies, like anti-EGFR pharmaceuticals (42). The combination of DCE-MRI and PET might therefore be particular helpful in studying the pharmacodynamics of response to such agents.

As in our prior study, we found a lack of correlation between FDG MR and blood flow, indicating that metabolism and blood flow may be poorly matched in LABC (11). We also found that FDG MR correlated poorly with DCE-MRI measures of peak SER and peak PE. The lack of correlation between DCE-MRI measures and FDG MR suggests that the positive correlation between blood flow and peak SER is not simply an artifact of tumor volume, position, or partial-volume effects that may impact image measures. In addition, the lack of correlation of FDG MR with blood flow suggests that $^{18}$F-FDG PET provides complementary metabolic information independent of vascular factors (10,11).

Our results agree with those of Brix et al who found no significant correlations between DCE-MRI pharmacokinetic parameters and $^{18}$F-FDG PET uptake in suspicious and malignant breast masses (43). The intracellular uptake of FDG is dependent on blood flow and vascular permeability as well as the cellular metabolism of glucose and intracellular trapping of

phosphorylated FDG (43). FDG MR measures may presumably correlate more closely with other metabolic markers such as magnetic resonance spectroscopy (MRS) measures of choline and lactate. However, preliminary investigations comparing MRS and PET measures in human tumors have been inconclusive, further illustrating inherent differences in the functional information provided by the two imaging modalities (44,45). Future studies in the breast with MRS, which we hope to perform, may shed more light on this issue.

### Limitations

The study is partly limited by the small sample size and the retrospective design. While we found strong correlation between PET measures of perfusion and peak SER, we did not see similar correlations between the PET measures and peak PE, a significant semi-quantitative measure of DCE-MRI kinetics. It is unclear why the correlations would be strong with peak SER but not peak PE. It may be a result of the small sample size. We are particularly interested in this question and are planning additional prospective studies with high temporal resolution DCE-MRI to answer it.

The retrospective nature of this study limits our DCE-MRI data to the protocols that emphasized high spatial resolution and low to moderate temporal resolution. Although the temporal resolution of our imaging technique did not lend itself to a complete pharmacokinetic analysis, we were able to differentiate low, medium, and high vascular permeability of tumors by the semi-quantitative DCE-MRI measures of peak PE and peak SER. These parameters were previously validated for stratifying risk of malignancy in clinical DCE-MRI evaluation and for assessing response to neoadjuvant therapy (20,24).

DCE-MRI obtained at higher temporal resolution enables full pharmacokinetic analysis of tumor blood flow, kinetic volume transfer constant (Ktrans), rate constant (Kep), coefficient of endothelial permeability (Kps) and can evaluate treatment response (10,13,14,16,17,25, 46–49). We plan to perform a prospective study with high temporal resolution DCE-MRI and full pharmacokinetic analysis in humans and compare it to $^{15}$O-water blood flow findings to improve our understanding of the tumor enhancement model and anti-vascular cancer therapies.

### Conclusions

Our findings in this exploratory analysis suggest that tumor perfusion, represented by $^{15}$O-water PET blood flow, is an important factor in the MRI enhancement dynamics of LABC. A lack of correlation of FDG MR with blood flow and DCE-MRI kinetics suggests that $^{18}$F-FDG PET provides complementary metabolic information independent of vascular factors.

## Acknowledgements

Supported by NIH Grants CA72064 and CA42045 and FHCRC CCSG Pilot Grant 015704

## References

1. Chen JH, Feig B, Agrawal G, et al. MRI evaluation of pathologically complete response and residual tumors in breast cancer after neoadjuvant chemotherapy. Cancer. 2007
2. Chen X, Moore MO, Lehman CD, et al. Combined use of MRI and PET to monitor response and assess residual disease for locally advanced breast cancer treated with neoadjuvant chemotherapy. Acad Radiol 2004;11:1115–1124. [PubMed: 15530804]
3. Daldrup-Link HE, Okuhata Y, Wolfe A, et al. Decrease in tumor apparent permeability-surface area product to a MRI macromolecular contrast medium following angiogenesis inhibition with correlations to cytotoxic drug accumulation. Microcirculation 2004;11:387–396. [PubMed: 15280064]

4. Jansson T, Westlin JE, Ahlstrom H, Lilja A, Langstrom B, Bergh J. Positron emission tomography studies in patients with locally advanced and/or metastatic breast cancer: a method for early therapy evaluation? J Clin Oncol 1995;13:1470–1477. [PubMed: 7751894]
5. Mankoff DA, Dunnwald LK, Gralow JR, et al. Blood flow and metabolism in locally advanced breast cancer: relationship to response to therapy. J Nucl Med 2002;43:500–509. [PubMed: 11937594]
6. Mankoff DA, Dunnwald LK, Gralow JR, et al. Changes in blood flow and metabolism in locally advanced breast cancer treated with neoadjuvant chemotherapy. J Nucl Med 2003;44:1806–1814. [PubMed: 14602864]
7. Martincich L, Montemurro F, De Rosa G, et al. Monitoring response to primary chemotherapy in breast cancer using dynamic contrast-enhanced magnetic resonance imaging. Breast Cancer Res Treat 2004;83:67–76. [PubMed: 14997056]
8. Partridge SC, Gibbs JE, Lu Y, et al. MRI measurements of breast tumor volume predict response to neoadjuvant chemotherapy and recurrence-free survival. AJR Am J Roentgenol 2005;184:1774–1781. [PubMed: 15908529]
9. Semple SI, Gilbert FJ, Redpath TW, et al. Correlation of MRI/PET rim enhancement in breast cancer: a delivery related phenomenon with therapy implications? Lancet Oncol 2003;4:759. [PubMed: 14662432]
10. Semple SI, Staff RT, Heys SD, et al. Baseline MRI delivery characteristics predict change in invasive ductal breast carcinoma PET metabolism as a result of primary chemotherapy administration. Ann Oncol 2006;17:1393–1398. [PubMed: 16788001]
11. Tseng J, Dunnwald LK, Schubert EK, et al. 18F-FDG kinetics in locally advanced breast cancer: correlation with tumor blood flow and changes in response to neoadjuvant chemotherapy. J Nucl Med 2004;45:1829–1837. [PubMed: 15534051]
12. Wahl RL, Zasadny K, Helvie M, Hutchins GD, Weber B, Cody R. Metabolic monitoring of breast cancer chemohormonotherapy using positron emission tomography: initial evaluation. J Clin Oncol 1993;11:2101–2111. [PubMed: 8229124]
13. Wasser K, Klein SK, Fink C, et al. Evaluation of neoadjuvant chemotherapeutic response of breast cancer using dynamic MRI with high temporal resolution. Eur Radiol 2003;13:80–87. [PubMed: 12541113]
14. Yu HJ, Chen JH, Mehta RS, Nalcioglu O, Su MY. MRI measurements of tumor size and pharmacokinetic parameters as early predictors of response in breast cancer patients undergoing neoadjuvant anthracycline chemotherapy. J Magn Reson Imaging 2007;26:615–623. [PubMed: 17729334]
15. Pham CD, Roberts TP, van Bruggen N, et al. Magnetic resonance imaging detects suppression of tumor vascular permeability after administration of antibody to vascular endothelial growth factor. Cancer Invest 1998;16:225–230. [PubMed: 9589031]
16. Wedam SB, Low JA, Yang SX, et al. Antiangiogenic and antitumor effects of bevacizumab in patients with inflammatory and locally advanced breast cancer. J Clin Oncol 2006;24:769–777. [PubMed: 16391297]
17. Wilmes LJ, Pallavicini MG, Fleming LM, et al. AG-013736, a novel inhibitor of VEGF receptor tyrosine kinases, inhibits breast cancer growth and decreases vascular permeability as detected by dynamic contrast-enhanced magnetic resonance imaging. Magn Reson Imaging 2007;25:319–327. [PubMed: 17371720]
18. Berg WA, Gutierrez L, NessAiver MS, et al. Diagnostic accuracy of mammography, clinical examination, US, and MR imaging in preoperative assessment of breast cancer. Radiology 2004;233:830–849. [PubMed: 15486214]
19. Bone B, Szabo BK, Perbeck LG, Veress B, Aspelin P. Can contrast-enhanced MR imaging predict survival in breast cancer? Acta Radiol 2003;44:373–378. [PubMed: 12846686]
20. Esserman L, Hylton N, George T, Weidner N. Contrast-Enhanced Magnetic Resonance Imaging to Assess Tumor Histopathology and Angiogenesis in Breast Carcinoma. Breast J 1999;5:13–21. [PubMed: 11348250]
21. Hylton NM. Vascularity assessment of breast lesions with gadolinium-enhanced MR imaging. Magn Reson Imaging Clin N Am 1999;7:411–420. [PubMed: 10382170]x

22. Knopp MV, Brix G, Junkermann HJ, Sinn HP. MR mammography with pharmacokinetic mapping for monitoring of breast cancer treatment during neoadjuvant therapy. Magn Reson Imaging Clin N Am 1994;2:633–658. [PubMed: 7489314]
23. Kuhl CK, Mielcareck P, Klaschik S, et al. Dynamic breast MR imaging: are signal intensity time course data useful for differential diagnosis of enhancing lesions? Radiology 1999;211:101–110. [PubMed: 10189459]
24. Li KL, Henry RG, Wilmes LJ, et al. Kinetic assessment of breast tumors using high spatial resolution signal enhancement ratio (SER) imaging. Magn Reson Med 2007;58:572–581. [PubMed: 17685424]
25. Padhani AR, Hayes C, Assersohn L, et al. Prediction of clinicopathologic response of breast cancer to primary chemotherapy at contrast-enhanced MR imaging: initial clinical results. Radiology 2006;239:361–374. [PubMed: 16543585]
26. Shames DM, Kuwatsuru R, Vexler V, Muhler A, Brasch RC. Measurement of capillary permeability to macromolecules by dynamic magnetic resonance imaging: a quantitative noninvasive technique. Magn Reson Med 1993;29:616–622. [PubMed: 8505897]
27. Knopp MV, Weiss E, Sinn HP, et al. Pathophysiologic basis of contrast enhancement in breast tumors. J Magn Reson Imaging 1999;10:260–266. [PubMed: 10508285]
28. Schelling M, Avril N, Nahrig J, et al. Positron emission tomography using [(18)F]Fluorodeoxyglucose for monitoring primary chemotherapy in breast cancer. J Clin Oncol 2000;18:1689–1695. [PubMed: 10764429]
29. Smith IC, Welch AE, Hutcheon AW, et al. Positron emission tomography using [(18)F]-fluorodeoxy-D-glucose to predict the pathologic response of breast cancer to primary chemotherapy. J Clin Oncol 2000;18:1676–1688. [PubMed: 10764428]
30. Wilson CB, Lammertsma AA, McKenzie CG, Sikora K, Jones T. Measurements of blood flow and exchanging water space in breast tumors using positron emission tomography: a rapid and noninvasive dynamic method. Cancer Res 1992;52:1592–1597. [PubMed: 1540969]
31. Beaney RP, Lammertsma AA, Jones T, McKenzie CG, Halnan KE. Positron emission tomography for in-vivo measurement of regional blood flow, oxygen utilisation, and blood volume in patients with breast carcinoma. Lancet 1984;1:131–134. [PubMed: 6140443]
32. Zasadny KR, Tatsumi M, Wahl RL. FDG metabolism and uptake versus blood flow in women with untreated primary breast cancers. Eur J Nucl Med Mol Imaging 2003;30:274–280. [PubMed: 12552346]
33. Goerres GW, Michel SC, Fehr MK, et al. Follow-up of women with breast cancer: comparison between MRI and FDG PET. Eur Radiol 2003;13:1635–1644. [PubMed: 12835979]
34. Muramoto S, Uematsu H, Sadato N, et al. H(2) (15)0 positron emission tomography validation of semiquantitative prostate blood flow determined by double-echo dynamic MRI: a preliminary study. J Comput Assist Tomogr 2002;26:510–514. [PubMed: 12218810]
35. Sakuma H, Koskenvuo JW, Niemi P, et al. Assessment of coronary flow reserve using fast velocity-encoded cine MR imaging: validation study using positron emission tomography. AJR Am J Roentgenol 2000;175:1029–1033. [PubMed: 11000158]
36. Ye FQ, Berman KF, Ellmore T, et al. H(2)(15)O PET validation of steady-state arterial spin tagging cerebral blood flow measurements in humans. Magn Reson Med 2000;44:450–456. [PubMed: 10975898]
37. Partridge SC, Heumann EJ, Hylton NM. Semi-automated analysis for MRI of breast tumors. Stud Health Technol Inform 1999;62:259–260. [PubMed: 10538368]
38. Sokoloff L, Reivich M, Kennedy C, et al. The [14C]deoxyglucose method for the measurement of local cerebral glucose utilization: theory, procedure, and normal values in the conscious and anesthetized albino rat. J Neurochem 1977;28:897–916. [PubMed: 864466]
39. Phelps ME, Huang SC, Hoffman EJ, Selin C, Sokoloff L, Kuhl DE. Tomographic measurement of local cerebral glucose metabolic rate in humans with (F-18)2- fluoro-2-deoxy-D-glucose: validation of method. Ann Neurol 1979;6:371–388. [PubMed: 117743]
40. Reivich M, Alavi A, Wolf A, et al. Glucose metabolic rate kinetic model parameter determination in humans: the lumped constants and rate constants for [18F]fluorodeoxyglucose and [11C] deoxyglucose. J Cereb Blood Flow Metab 1985;5:179–192. [PubMed: 3988820]

41. Reivich M, Kuhl D, Wolf A, et al. The [18F]fluorodeoxyglucose method for the measurement of local cerebral glucose utilization in man. Circ Res 1979;44:127–137. [PubMed: 363301]

42. Su H, Bodenstein C, Dumont RA, et al. Monitoring tumor glucose utilization by positron emission tomography for the prediction of treatment response to epidermal growth factor receptor kinase inhibitors. Clin Cancer Res 2006;12:5659–5667. [PubMed: 17020967]

43. Brix G, Henze M, Knopp MV, et al. Comparison of pharmacokinetic MRI and [18F] fluorodeoxyglucose PET in the diagnosis of breast cancer: initial experience. Eur Radiol 2001;11:2058–2070. [PubMed: 11702142]

44. Alger JR, Frank JA, Bizzi A, et al. Metabolism of human gliomas: assessment with H-1 MR spectroscopy and F-18 fluorodeoxyglucose PET. Radiology 1990;177:633–641. [PubMed: 2243962]

45. Luyten PR, Marien AJ, Heindel W, et al. Metabolic imaging of patients with intracranial tumors: H-1 MR spectroscopic imaging and PET. Radiology 1990;176:791–799. [PubMed: 2389038]

46. Brix G, Kiessling F, Lucht R, et al. Microcirculation and microvasculature in breast tumors: pharmacokinetic analysis of dynamic MR image series. Magn Reson Med 2004;52:420–429. [PubMed: 15282828]

47. Hayes C, Padhani AR, Leach MO. Assessing changes in tumour vascular function using dynamic contrast-enhanced magnetic resonance imaging. NMR Biomed 2002;15:154–163. [PubMed: 11870911]

48. Pickles MD, Lowry M, Manton DJ, Gibbs P, Turnbull LW. Role of dynamic contrast enhanced MRI in monitoring early response of locally advanced breast cancer to neoadjuvant chemotherapy. Breast Cancer Res Treat 2005;91:1–10. [PubMed: 15868426]

49. Thukral A, Thomasson DM, Chow CK, et al. Inflammatory breast cancer: dynamic contrast-enhanced MR in patients receiving bevacizumab--initial experience. Radiology 2007;244:727–735. [PubMed: 17709827]

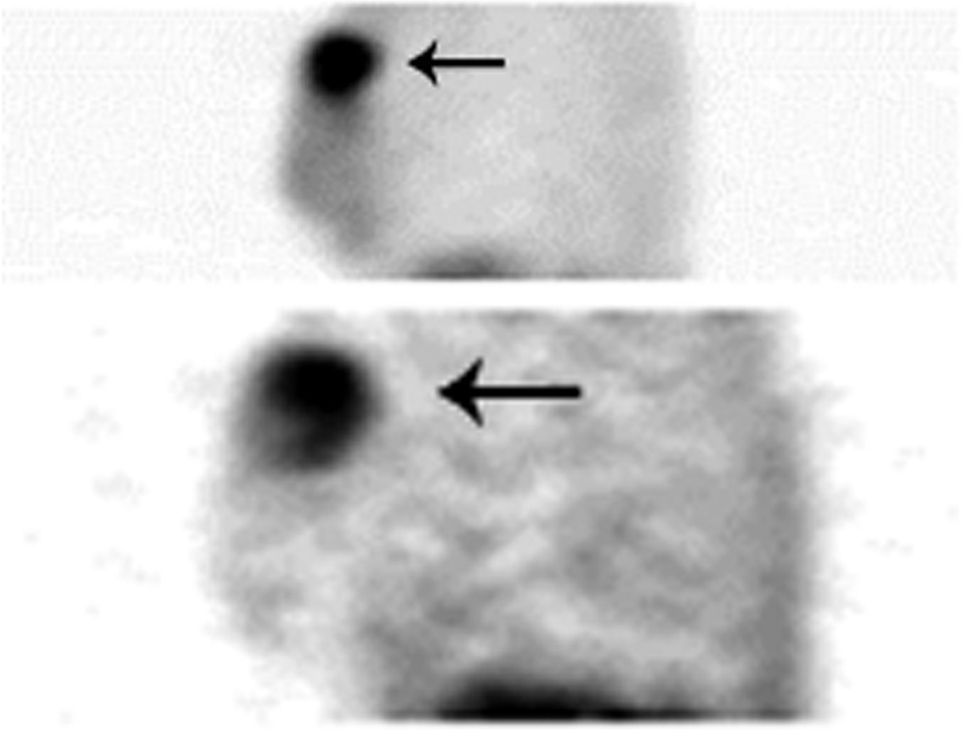

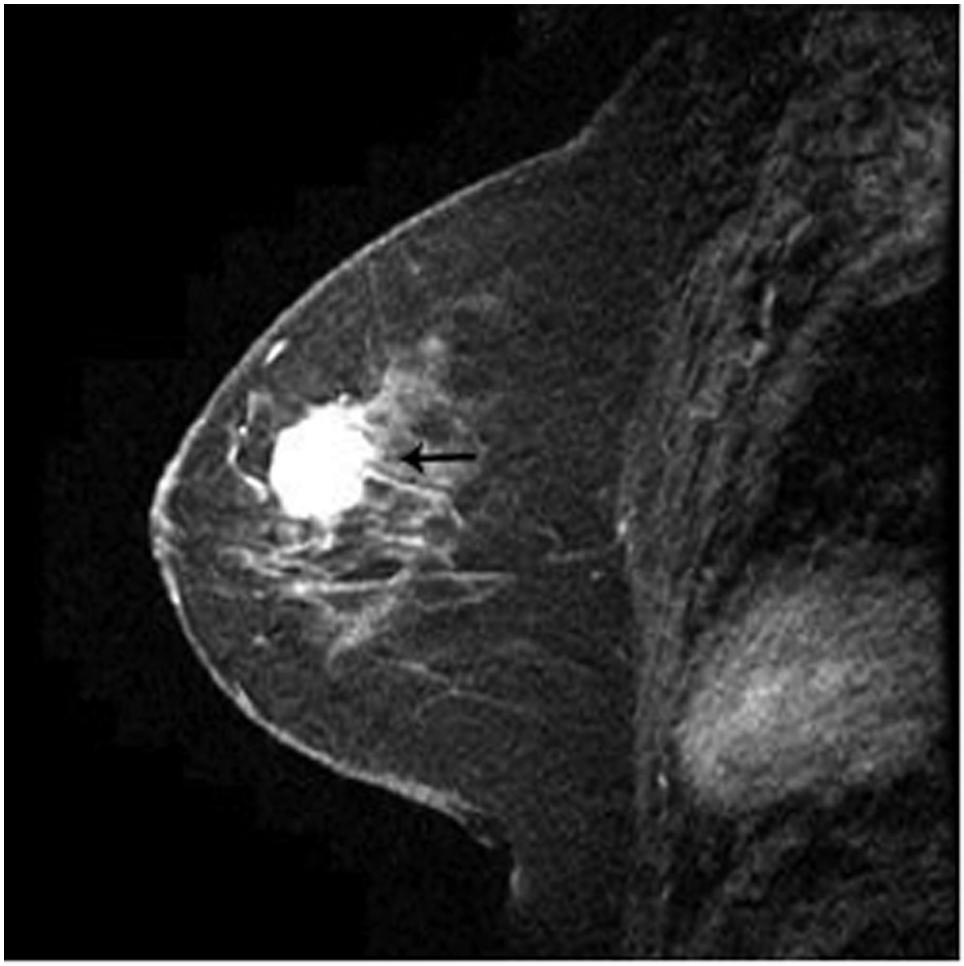

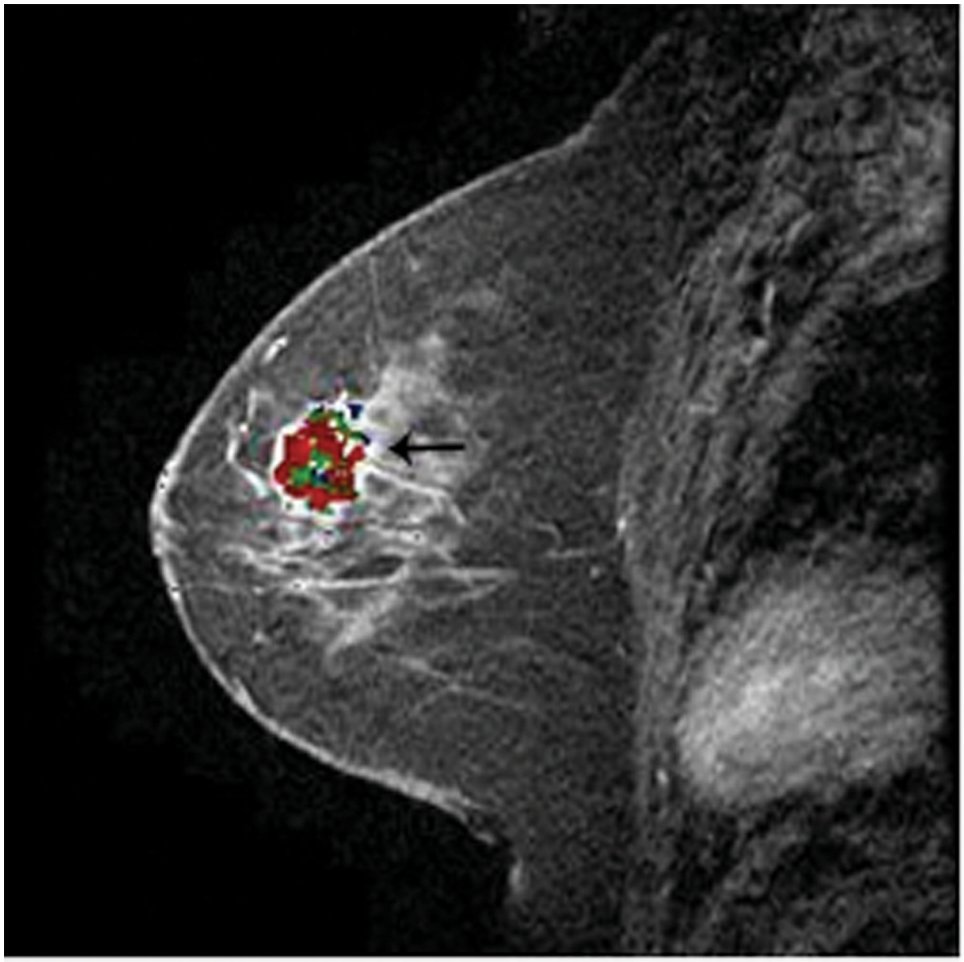

**Figure 1.**

Figure 1a. $^{18}$F-FDG PET sagittal image of the breast demonstrates radiotracer uptake in the tumor (arrow) indicating high metabolism.

Figure 1b. $^{15}$O-water PET sagittal image of the breast demonstrates radiotracer (arrow) that indicates blood flow in the tumor in a slightly different distribution than the metabolism of $^{18}$F-FDG.

Figure 1c. DCE-MRI sagittal post contrast fat-suppressed T1 image of the breast demonstrates avid enhancement of the tumor (arrow).

Figure 1d. DCE-MRI sagittal post contrast fat-suppressed T1 image of the breast demonstrates the color map of SER values overlayed on the tumor. Red corresponds to SER values >1.1 (washout), green Corresponds to SER values of 0.9–1.1 (plateau) and blue corresponds to SER values <0.9 (persistent).

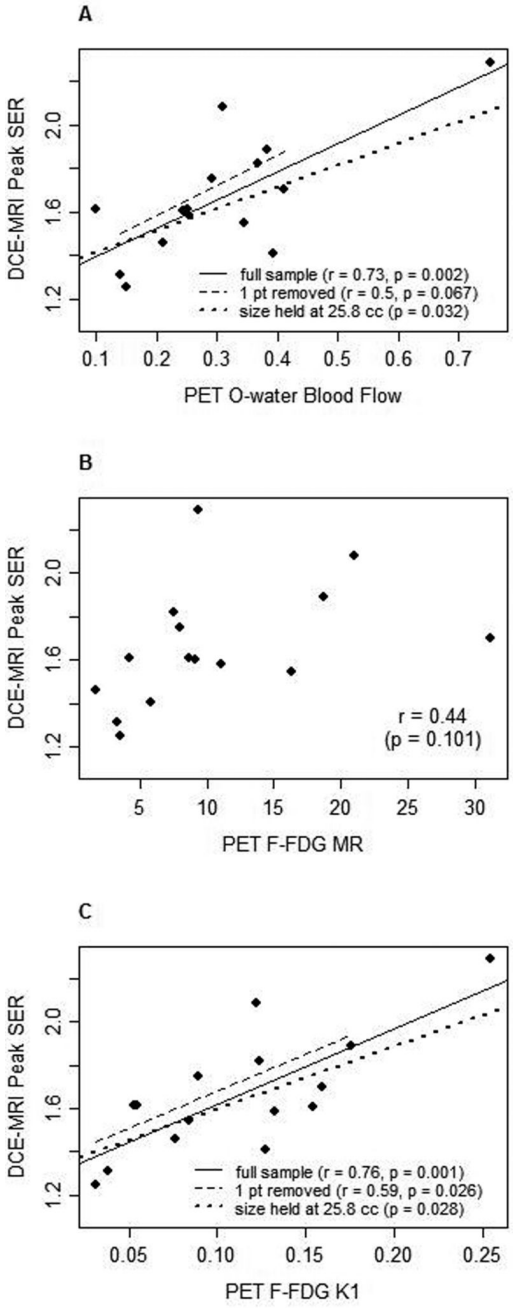


**Figure 2.**

Bivariate scatterplots of DCE-MRI peak SER with A. PET$^{15}$O-water blood flow (mL/min/g), B. $^{18}$F-FDG MR, (μmole/min/100g) and C. $^{18}$F FDG $K_1$ (mL/min/g), n=15. 2A and 2C contain multiple fits to demonstrate the full sample (solid line), the full sample with the one highest SER patient removed (dashed line) and the full sample controlled for tumor size (dotted line).

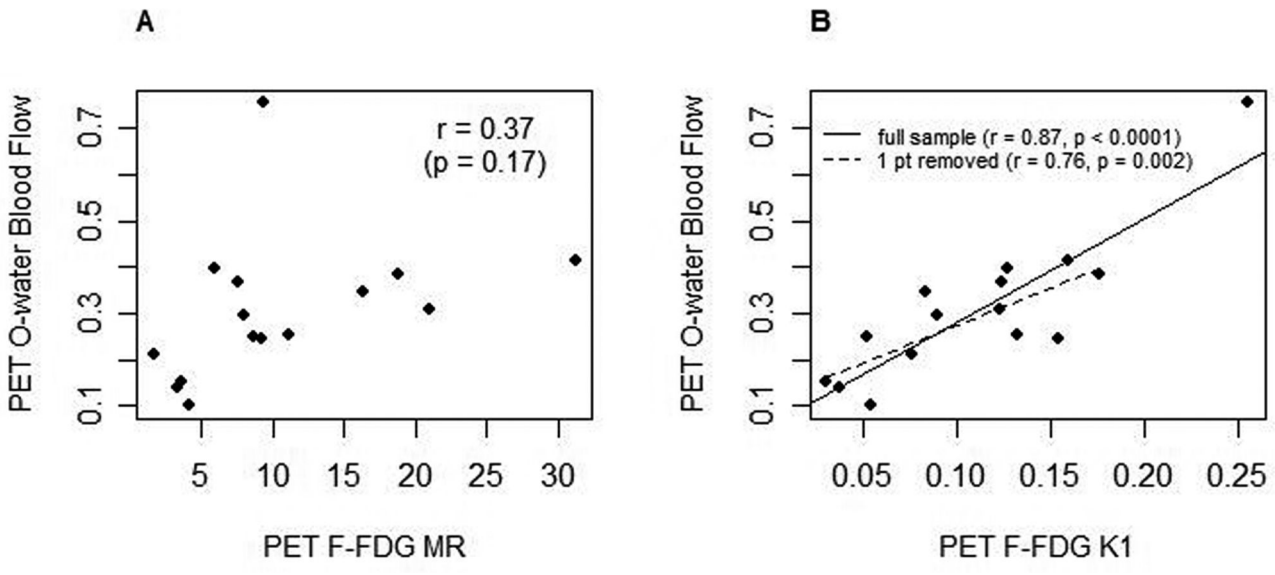


**Figure 3.**

Bivariate scatterplots of PET $^{15}$O-water blood flow (mL/min/g) with A. $^{18}$F-FDG MR (μmole/min/100g) and B. $^{18}$F-FDG $K_1$ (mL/min/g), n=15. 3B includes two fits to demonstrate the full sample (solid line) and the full sample with the one highest blood flow patient removed (dashed line).

**Table 1**

Correlations between PET and DCE-MRI variables.

| DCE-MRI variables | $^{15}$O-water PET Blood Flow | $^{18}$F-FDG PET MR | $^{18}$F-FDG PET $K_1$ |
|---|---|---|---|
| Peak SER | R=0.73 (p=0.002) | R=0.44 (p=0.10) | R=0.76 (p=0.001) |
| Peak PE | R=0.28 (p=0.30) | R=0.15 (p=.59) | R=0.30 (p=0.28) |